Desalination and Water Treatment
www.deswater.com
doi: 10.5004/dwt.2022.28486

262 (2022) 227–234
June

Efficient Rhodamine B degradation with molybdenum disulfide nano-flowers as monopersulfide activator under varying precursor solution pH

Mengxi Li, Yinghua Li*, Ruibin Nan, Wenyue Yin, Lijun Chen, Jingwen Zhang, Lu Liu, Chaoqun Zhu

School of Resources and Civil Engineering, Northeastern University, Shenyang 110819, China, Tel. +86-24-13940237668; email: liyinghua1028@126.com (Y. Li), Tel. +86-24-18735559135; email: 1044080844@qq.com (M. Li), Tel. +86-24-15776585411; email: 1925490782@qq.com (R. Nan), Tel. +86-24-18842587163; email: 1024864335@qq.com (W. Yin), Tel. +86-24-18842414380; email: 18621831004@163.com (L. Chen), Tel. +86-24-15566287898; email: 1742494215@qq.com (J. Zhang), Tel. +86-24-15724360733; email: 1017477714@qq.com (L. Liu), Tel. +86-24-18754811887; email: zcq6572509@163.com (C. Zhu)

Received 29 October 2021; Accepted 9 April 2022

ABSTRACT

Molybdenum disulfide (MoS_2) nano-flowers were prepared with different physicochemical properties resulting from varying precursor pH. The degradation rate of Rhodamine B (RhB) via MoS_2-activated monopersulfide (PMS) was investigated under the synergy of light. The results showed that the prepared MoS_2 at pH 1, 2, 3 and 4 were stable 2H-MoS_2 and flowery. The size was evenly distributed between 200 and 500 nm. The degradation rates of RhB by MoS_2 activated PMS were improved from 12.85% to 31.25% comparing with that of PMS alone under 120 min of light. Among them, MoS_2-2 (pH 2) presented the highest activation efficiency. Its specific surface area reached 40.012 m^2/g, and the removal rate of RhB was as high as 63.73%. Although MoS_2-1 (pH 1) had the largest specific surface area (69.622 m^2/g), the removal of RhB decreased to 58.56% due to its undesirable crystallinity. The main active substances of MoS_2 activated PMS were –OH and $SO_4^{-\bullet}$ under the synergy of light.

Keywords: Multilayer structure; Nanocrystalline materials; Molybdenum disulfide; Precursor pH; Peroxymonosulfate; Activation efficiency

1. Introduction

Sulfate radicals ($SO_4^{-\bullet}$) have a relatively wider pH tolerance range (2–10 vs. 2–4), higher redox potential (E_0 2.5–3.1 V vs. E_0 1.8–2.7 V), and longer half-life (4 s vs. 0.1 μs) than hydroxyl radicals (–OH). Therefore, persulfate is able to treat refractory organic wastewater [1–3]. The prerequisite is the need to excite the peroxide bond –O–O– breaking with the help of transition metals, electricity, light or heat [4–6] to produce $SO_4^{-\bullet}$ and fully exploit its oxidative properties.

Molybdenum disulfide (MoS_2) is a layered transition metal sulfide with a stable semiconductor crystal structure. The nanostructures have unsaturated dangling bonds on the surface to induce electron transfer under light. Therefore, MoS_2 exhibits excellent catalytic degradation of organic matter [7]. Recent studies on MoS_2-catalyzed monopersulfide (PMS) focused on the control of MoS_2 morphology, solution pH, dosing amount, etc. Zhou et al. [8] used bulk MoS_2 to activate PMS and found that neither single MoS_2 nor PMS could achieve the degradation of carbamazepine (CBZ). The kinetic model showed that the degradation of bisphenol A (BPA) via ce-MoS_2/PMS was almost 150 times higher than that of the bulk MoS_2/PMS [9]. Sheng et al. [10] synthesized a composite photocatalyst to activate PMS and found that doping with 20 wt.% MoS_2 resulted in an increase in specific surface area of 62.4 m^2/g.

* Corresponding author.

In the exploration of MoS_2-catalyzed PMS, the adsorption capacity of the active ingredient determines the rate of radical production [9], and the precursor pH significantly affects the physicochemical properties of MoS_2, such as specific surface area, activation sites and crystallinity, thereby affecting the generation of free radicals. However, the activation capacity of MoS_2/PMS has not been investigated in depth.

In this study, thin layers of MoS_2 with different physicochemical properties were prepared by precisely controlling the pH (1, 2, 3 and 4) of the precursor solution. The effect of precursor pH on the degradation rate of Rhodamine B (RhB) was investigated under the synergy of natural light. Finally, the mechanism of contaminant degradation by MoS_2/PMS based on the pH regulation was analyzed.

2. Materials and methods

2.1. Reagents

Thiourea (CH_4N_2S) was bought from Beilian Fine Chemicals Development Co. Sodium molybdate ($Na_2MoO_4 \cdot 2H_2O$) was obtained from Zhiyuan Chemical Reagent Co. Potassium persulfate ($K_5H_3S_4O_{18}$) was purchased from Macklin reagent Co., Ltd. Rhodamine B ($C_{28}H_{31}CN_2O_3$) was obtained from Reagent Research Institute which selected as the major organic pollutant in water. P-benzoquinone (BQ, purity ≥ 99%) was bought from Macklin reagent Co., Ltd. Pharmaceuticals from other companies will also be used, including oxalic acid ($H_2C_2O_4$), hydrochloric acid (HCl), methanol (CH_4O, purity ≥ 99.5%) and tert-butanol ($C_4H_{10}O$, purity ≥ 99.5%). All chemicals were used as received without further purification, and all solutions were prepared with deionized water.

2.2. Synthesis of MoS_2 nano-particles

MoS_2 nano-particles were fabricated by a hydrothermal method. First, a certain amount of powder mixture of sodium molybdate and thiourea with molar ratio of 1:3 was used as the precursor (0.726 g of sodium molybdate and 0.685 g of thiourea) and dissolved in 35 mL of deionized water, and oxalic acid was added as surfactant. Second, the pH of the precursor solution was adjusted to 1, 2, 3 and 4 in order using concentrated hydrochloric acid. Then the mixed solution was transferred into a stainless 50 mL Teflon-lined autoclave, sealed and kept at 220°C for 24 h. The precipitates were washed three times with deionized water and anhydrous ethanol respectively after precipitates were cooled to room temperature. Finally, the collected black precipitate was dried for 8 h. The resulting samples were labeled as MoS_2-1, MoS_2-2, MoS_2-3 and MoS_2-4, respectively.

2.3. Analytical method

The surface morphological details of the bulk MoS_2 were scanned by scanning electron microscope (SEM, Hitachi S4800, acceleration voltage 0.1 V–30 kV). The crystal structure was characterized by X-ray diffraction (XRD, X Pertpro, Panalytical, Netherlands, with a maximum power of 3 KW. Copper target as target material, scanning range 5°–90°, scanning speed 12°/min). Surface area (SA) were calculated by N_2 adsorption/desorption using an automatic adsorption instrument (ASAP2020HD88, Mike, USA). Using monochromatic Al Kα radiation (1486.6 eV, 12 kV) as the X-ray source, the elemental composition and chemical state of the sample were analyzed by X-ray photoelectron spectroscopy (XPS, Thermo Scientific K-Alpha).

UV visible diffuse reflectance spectroscopy (DRS) was measured by a Shimadzu UV-3600 spectrophotometer and different Mo material was used as the reference to analyze the visible light absorption characteristics of samples. The residual RhB concentration was measured using a UV–Vis spectrophotometer (UV3600, SHI-MADZU). The metal leaching of molybdenum was measured by inductively coupled plasma–mass spectrometry (ICP–MS, EXPEC7000, Spotlight Technology Co., China).

2.4. Photocatalytic experiment

For RhB degradation experiments, a 350 W cold light source xenon lamp was used to simulate solar light source for photocatalytic experiments, full spectral range. 15 mg/L of Rhodamine solution was used as the target pollutant. 12 mg of photocatalyst was dispersed in 80 mL of 48 mmol/L rhodamine contaminants. As soon as the desired amount of MoS_2 powder and PMS was added into the solution simultaneously with a constant stirring speed of 500 rpm, the timekeeping began. Dark reaction was carried out for 30 min to achieve adsorption-resolution equilibrium between sample and contaminant. The reaction solution was then placed in a dark box with magnetic stirring under light, and 3.5 mL of sample was taken every 20 min after high-speed centrifugation (10,000 rpm). The absorbance of the obtained suspension was measured at 554 nm. The degradation rate (D) of RhB solution was calculated according to the following equation: $D = (C_0 - C)/C_0 = (A_0 - A)/A_0$, where A_0 and C_0 were the absorbance and concentration of RhB solution at the initial time, while A_t and C_t were the absorbance and concentration of RhB solution at the reaction time, respectively.

3. Results and discussion

3.1. Characterization

The morphological characteristics of MoS_2 before and after pH adjustment are shown in Fig. 1a–d. The size of MoS_2 distributed in the range of 200–500 nm. The nanosheets were stacked together and showed a flower-like structure. MoS_2 was thin and clearly visible at the edges. It could be seen from Fig. 1e and f that the material was composed of S and Mo elements with uniform distribution.

XRD was also performed to investigate the crystal phase composition of MoS_2 under different pH preparation conditions. As shown in Fig. 2 several typical sharp and narrow diffraction peaks for 2H MoS_2 were observable in 13.95°, 33.03°, 39.38° and 58.33° correspond well to the Bragg planes of (002), (100), (103) and (110). The positions of the diffraction peaks were consistent with the standard card match of 2H-MoS_2 (JCPDS-PDF: 650160). It is worth noting that the intensity of each diffraction peak of MoS_2-1 was significantly lower than that of MoS_2-2, MoS_2-3 and

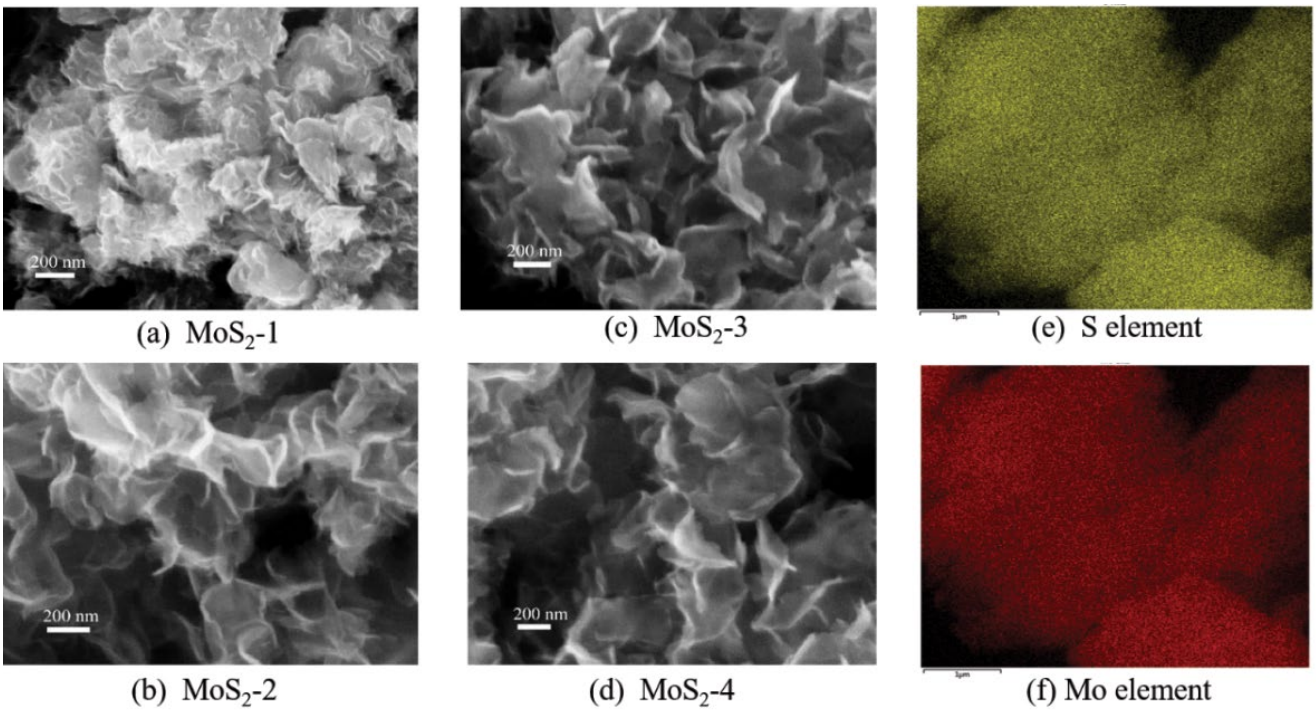

Fig. 1. SEM of MoS_2 before and after pH adjustment (a–d); SEM mapping images of MoS_2: (e) S, (f) Mo.

MoS_2-4, especially the growth of the (002) crystal plane. The relatively poor crystallization properties and low purity of MoS_2-1 were indicated. The BET surface area were 69.622, 40.012, 32.104 and 24.097 m^2/g for MoS_2-1, MoS_2-2, MoS_2-3 and MoS_2-4 respectively. Unsurprisingly MoS_2-1 has the largest specific surface area which may be related to the presence of a large number of defects on its surface. This result was verified in the above characterization.

XPS was applied to investigate the surface state changes of precursor MoS_2 at different pH values. The binding energy of all XPS spectra was calibrated by C1s at 284.8 eV. The XPS survey spectrum of MoS_2 further evidenced the presence of Mo, S, C and O elements (Fig. 3a–d), while the presence of O element may be caused by air exposure [11]. Through calculating peak area, the atom ratio of Mo and S was about 1:2. In summary, the above results further confirmed the fact that the tested samples were composed of MoS_2. The XPS Mo 3d core-level spectrum (Fig. 3e–h) could be curve-fitted into three main peak components. First, the peak at 226.3 eV corresponds to S 2s. Second, the main peaks at 229.2 eV and 232.5 eV which are the characteristics of MoS_2 could be attributed to Mo $3d_{5/2}$ and Mo $3d_{3/2}$, respectively [12]. These two main peaks indicated that most of the Mo existed in the state of Mo(IV). The other peak centered at 235.9 eV was assigned to Mo^{6+} states [13]. No new phase appears in the XRD pattern, implying no formation of oxides such as MoO_3 [14]. From Fig. 3e–h, by split-peak fitting, it was observed that there were different valence states of Mo present in the materials prepared with different pH precursors. This is mainly because the reactant Mo ions exist in different forms at different pH values, affecting the formation of MoS_2 [15]. Indicating that the pH indeed changed the reduction degree of Mo which might influence the catalytic performance. After adjusting pH, the amount of Mo(VI) reduced from 4-Mo (0.05%) to 1-Mo (5.68%). demonstrating the state transformation between Mo(IV) and Mo(VI) and the process may be interpreted as the specific effect of MoO_4^{2-} ions tends to polymerize under acidic conditions, and the existence state of Mo^{6+} ions in solution thus depends on the degree of polymerization of Mo^{6+} ions.

3.2. Photocatalytic activity

Fig. 4a is a graph showing the performance of MoS_2 photocatalyst on RhB degradation under different pH conditions of precursor fluids preparation. The removal rate of RhB by single PMS was low, only 32.87% after 120 min of operation. However, the degradation was significantly improved after the addition of MoS_2. 64.02% removal of RhB was achieved by MoS_2-2/PMS system. The removal rates were 55.42% and 45.72% for MoS_2-3/PMS and MoS_2-4/PMS, respectively.

MoS_2-2, MoS_2-3 and MoS_2-4 were flower-like, and insignificant difference existed in crystallinity (Fig. 2). The different removal efficiency may be due to the difference in specific surface area. On the one hand, a larger specific surface area means that the Mo was more fully exposed and had more edge active sites per unit volume, which in turn led to a higher efficiency of electron transfer [16] and a significantly enhanced activation effect. On the other hand, the larger specific surface area also provided sufficient active sites [17]. However, for MoS_2-1, the removal rate of RhB was only 58.56%. Obviously, the maximum specific surface area of MoS_2 did not produce

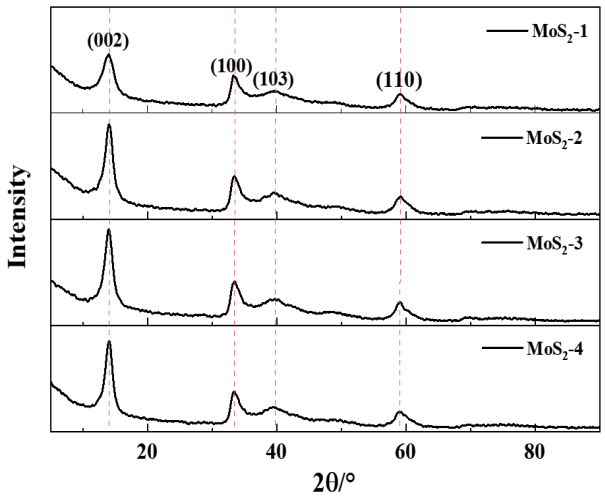

Fig. 2. XRD MoS_2 patterns of under different pH preparation conditions.

the best activation effect because the Mo-O bond in MoO_4^{2-} was weak and easily replaced by S^{2-}. MoO_4^{2-} was then easily dehydrated under the condition of strong acid (pH 1) to produce polymolybdate, which inhibited the formation of MoS_2 and led to its undesirable crystallinity [18] (Fig. 2).

3.3. Radical scavenging experiments

To clarify the types of active free radicals, CH_4O, TBA and BQ were used as radical quenchers (Fig. 4b). At specified intervals, a 3.5 mL of samples was filtered through a 0.45 μm PTFE syringe filter before analysis. Previous studies showed that CH_4O can quench both $SO_4^{-\bullet}$ and –OH, while TBA can quench more quickly with –OH [19]. After the addition of methanol and tert-butanol, the degradation rates of RhB was 28.26% and 43.58% lower compared to the control, respectively. The 15.32% difference may be resulted from the $SO_4^{-\bullet}$ involved in the degradation. In summary, in the MoS_2/PMS activation system, –OH and $SO_4^{-\bullet}$ were involved as the main ROS.

3.4. Cycle performance test

As shown in Fig. 5, under the full-spectrum xenon lamp irradiation, it was found that the degradation rate of rhodamine under light conditions was decreasing rapidly with a trend of about 3% after three cycles of experiments. A possible explain to this drawback could be that recycled MoS_2 surfaces clogged with contaminant molecules. In addition, the presence of losses during the recycling of collected materials could also lead to a decrease in the degradation rate of contaminants. Besides, it has been shown that PMS has little ability to reduce Mo species in the highly oxidized state [20].

3.5. Dissolution of MoS_2 nanosheets

It has been found that MoS_2 nanosheets are susceptible to oxidation under environmental conditions resulting in the release of soluble molybdenum species, which may cause secondary contamination [21]. The Mo ion release from MoS_2 nanosheets prepared with different pH precursors was evaluated in deionized water. For dissolution experiments, different MoS_2 nanosheets at 10 mg/L were prepared in deionized water. Samples were collected at 12, 24, 48 and 72 h. At each sampling time, the collected suspensions were centrifuged (30 mL, 5 min) to separate the MoS_2 nanosheets and the dissolved Mo ions. Then filtered through a 0.45 um pore size membrane for further solid-liquid separation. As shown in Fig. 6, after 72 h exposure under natural conditions, the metal leaching rates of Mo were 0.56 mg/L (MoS_2-1), 0.70 mg/L (MoS_2-2), 0.64 mg/L (MoS_2-3), 0.09 mg/L (MoS_2-4), respectively. It indicates that the dissolved amount is relatively low and not enough to cause secondary pollution to the environment. However, MoS_2-2 has a higher dissolution than the rest of different pH, which is more favorable for its participation in the activation of PMS to degrade the pollutants. This is consistent with the above experimental results.

3.6. Possible activation mechanism

The results suggested that PMS generated more ROS under the co-excitation of light and MoS_2 (Fig. 4b). The activation mechanism can be divided into two parts (Fig. 7). First, the UV-vis diffuse absorption spectra indicated that four MoS_2 species showed strong visible light absorption properties. This was related to their narrow band gap width (1.3–1.9 eV). Under ultraviolet (UV) irradiation, the O–O bond in PMS broke and converted PMS to $SO_4^{-\bullet}$ and –OH [22]. Zhou et al. [23] showed by DFT simulations that the reaction between PMS and BPR could take place spontaneously and a large amount of charge would accumulate on the surface of PMS, and the increase in the bond length of O–O bond implies a breakage tendency which indicates that PMS will undergo strong electron transfer with BPR. In addition, under the excitation of visible light, MoS_2 generated photogenerated electrons that reacted with HSO_5^- to form $SO_4^{-\bullet}$ [24]. Next, Mo(IV) produced by the dissociation of MoS_2 underwent electron transfer with HSO_5^- to produce Mo(V) and $SO_4^{-\bullet}$. Following that, Mo(V) continued to undergo electron transfer with HSO_5^- to produce Mo(VI) and $SO_4^{-\bullet}$ [Eqs. (1)–(6)]. Finally, the reduction of Mo(VI) to Mo(IV) by PMS is slow [8]. In the MoS_2/PMS system, Mo underwent a complete redox process with continuous production of $SO_4^{-\bullet}$ [25]. Different precursor pH created the varying specific surface area, crystallinity and number of active sites of MoS_2, resulting in different activation performance and degradation ability of PMS.

$$HSO_5^- + h\upsilon \rightarrow SO_4^{-\bullet} + {}^{\bullet}OH \quad (1)$$

$$MoS_2 + h\upsilon \rightarrow e^- + h^+ \quad (2)$$

$$e^- + HSO_5^- \rightarrow SO_4^{-\bullet} + OH^- \quad (3)$$

$$Mo(IV) + HSO_5^- \rightarrow Mo(V) + SO_4^{-\bullet} + OH^- \quad (4)$$

$$Mo(V) + HSO_5^- \rightarrow Mo(IV) + SO_4^{-\bullet} + OH^- \quad (5)$$

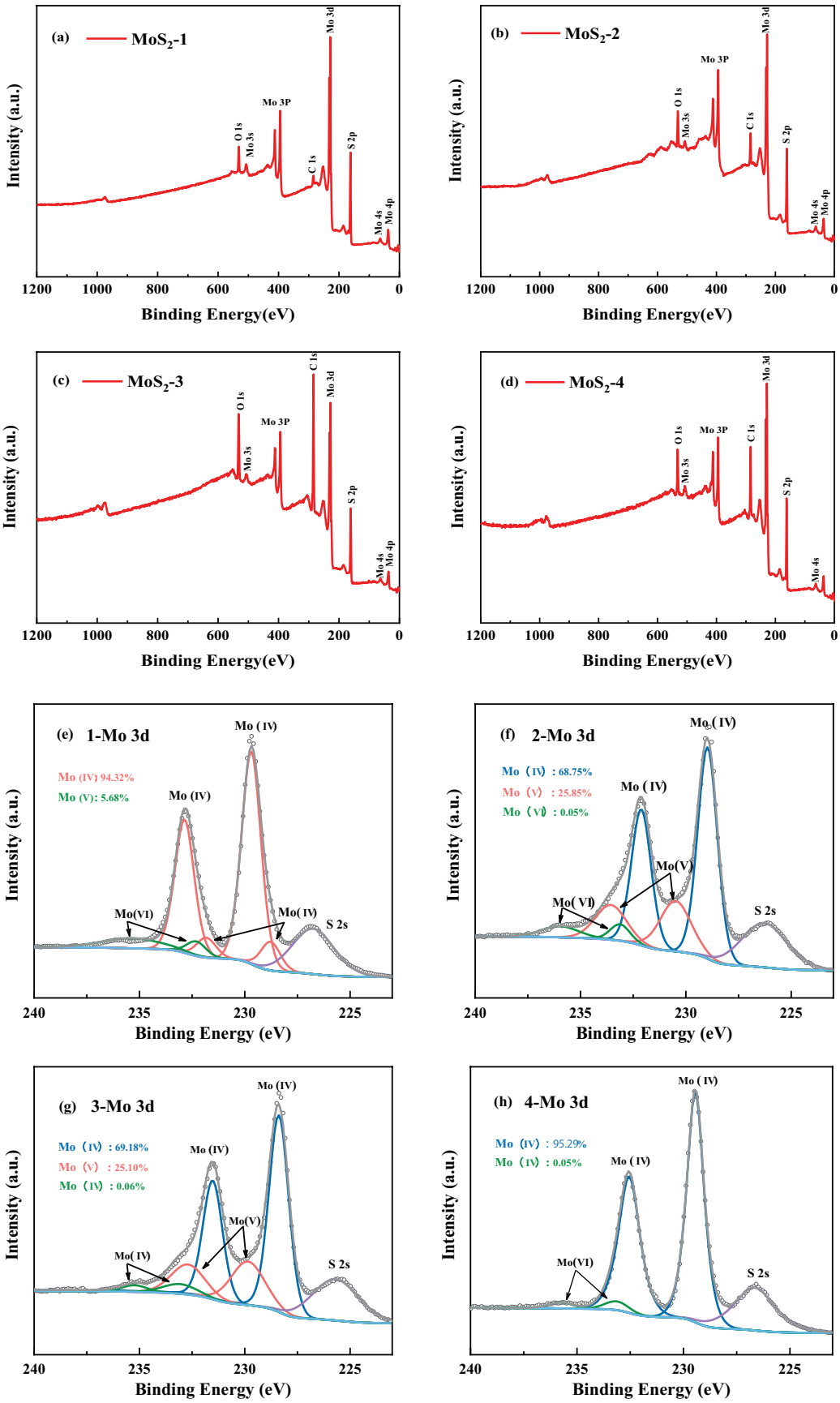

Fig. 3. XPS survey spectra of MoS_2 in different pH precursors (a–d), Mo 3d core-level spectra of MoS_2 (e–h).

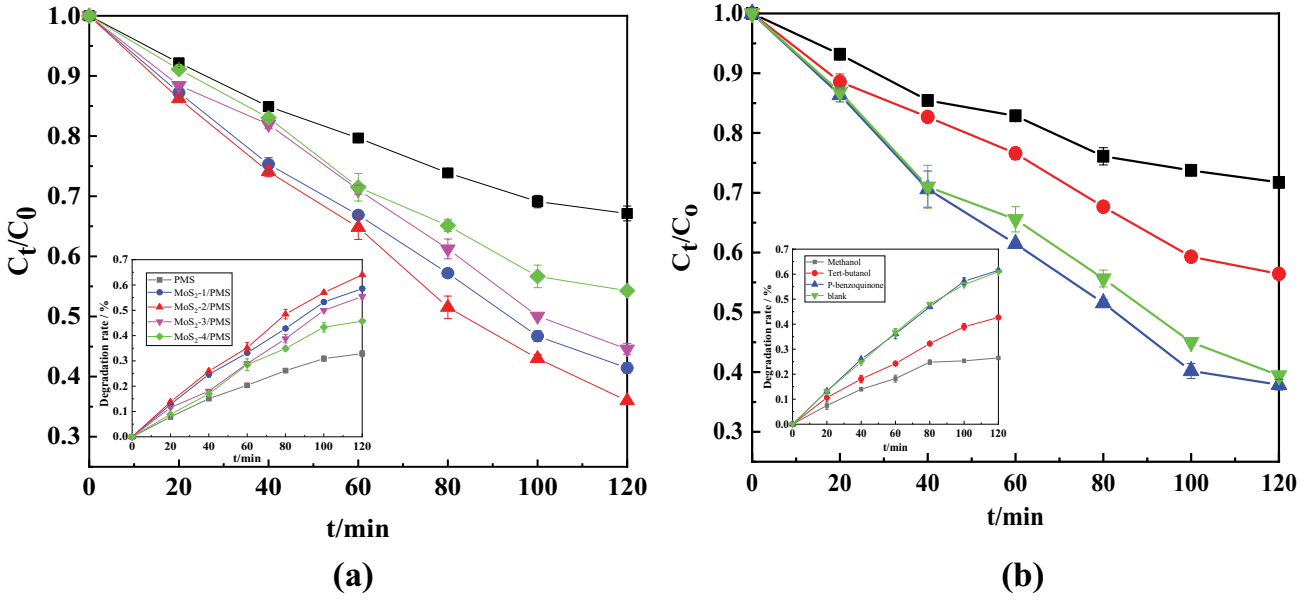

Fig. 4. Influence of different MoS_2 on the degradation of RhB (a) and photocatalytic degradation effect of MoS_2/PMS system under different scavengers (b). Experiment conditions: $[RhB]_0$ = 15 mg/L; $[MoS_2]$ = 0.125 g/L; [PMS] = 0.15 g/L; under 350 W xenon lamp light.

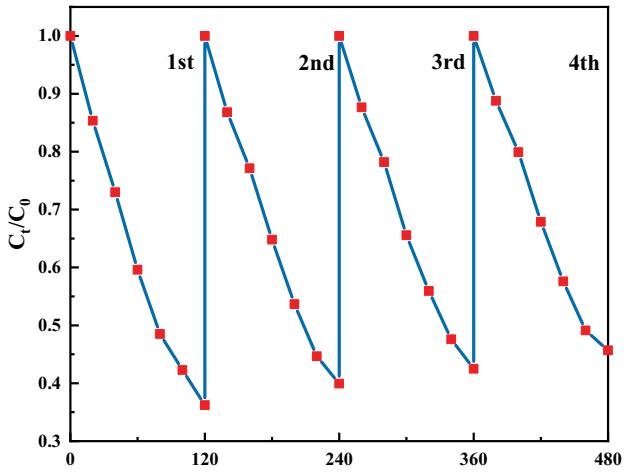

Fig. 5. Stability test for MoS_2 after 4 circles. Experiment conditions: $[RhB]_0$ = 15 mg/L; $[MoS_2]$ = 0.125 g/L; [PMS] = 0.15 g/L; under 350 W xenon lamp light.

$$Mo(VI) + 2HSO_5^- \rightarrow Mo(IV) + 2SO_5^{-\bullet} + H^+ \quad (6)$$

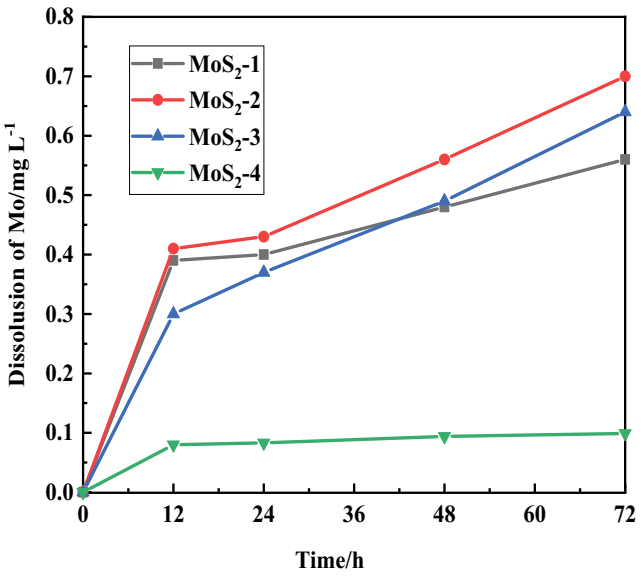

Fig. 6. Dissolution of MoS_2 nanosheets in different pH in water solution. Experiment conditions: $[MoS_2]$ = 0.01 g/L; under natural light conditions.

4. Conclusion

MoS_2 with different physicochemical properties were prepared by controlling the pH of precursor solution. The results showed that the MoS_2 prepared at different pH values were flower-like. The specific surface areas were MoS_2-1 (pH 1) > MoS_2-2 (pH 2) > MoS_2-3 (pH 3) > MoS_2-4 (pH 4). Meanwhile, the light absorption ability was MoS_2-1 > MoS_2-2 > MoS_2-3 > MoS_2-4. The removal rates of RhB were 58.56%, 64.02%, 55.42% and 45.72% for MoS_2-1/PMS, MoS_2-2/PMS, MoS_2-3/PMS and MoS_2-4/PMS, respectively, which were 12.85% to 31.25% higher than that of PMS alone. The ROS types mainly included –OH and $SO_4^{-\bullet}$. Under the irradiation of natural light for 120 min, the highest performance was found for MoS_2-2/PMS due to its desirable crystallinity, specific surface area and excellent dissolution rate. The results indicate that the regulation of precursor solution pH is an effective way to enhance the degradation ability of MoS_2/PMS.

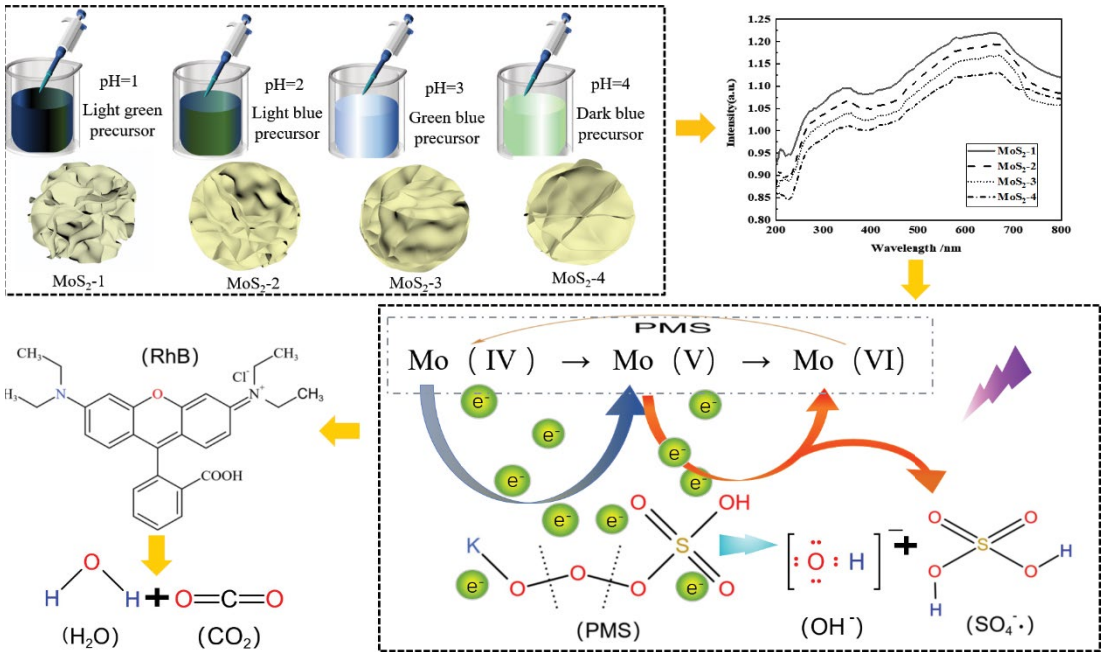

Fig. 7. Mechanism of PMS activation and degradation of organic matter.

CRediT authorship contribution statement

Mengxi Li: Conceptualization, Validation, Experimental section, Writing – original draft. Yinghua Li: Project administration, Funding acquisition, Supervision, Review & editing. Ruibin Nan: Data curation, Data analysis, Validation. Wenyue Yin: Writing – review & editing, Software. Lijun Chen: Conceptualization, Datacuration. Jingen Zhang: Validation, Software. Lu Liu: Writing – review & editing. Chaoqun Zhu: Formal analysis, Visualization.

Declaration of competing interest

The authors declare that they have no known competing financial interests or personal relationships that could have appeared to influence the work reported in this paper.

References

[1] Z. Liu, R.D. Su, X. Sun, W.Z. Zhou, B.Y. Gao, Q.Y. Yue, Q. Lia, The obvious advantage of amino-functionalized metal-organic frameworks: as a persulfate activator for bisphenol F degradation, Sci. Total Environ., 741 (2020) 140464, doi: 10.1016/j.scitotenv.2020.140464.

[2] J.L. Wang, S.Z. Wang, Activation of persulfate (PS) and peroxymonosulfate (PMS) and application for the degradation of emerging contaminants, Chem. Eng. J, 334 (2018) 1502–1517.

[3] L.D. Lai, P. Zhou, H.Y. Zhou, M. Sun, Y. Yuan, Y. Liu, G. Yao, B. Lai, Heterogeneous Fe(III)/Fe(II) circulation in $FeVO_4$ by coupling with dithionite towards long-lasting peroxymonosulfate activation: pivotal role of vanadium as electron shuttles, Appl. Catal., B, 297 (2021) 120470, doi: 10.1016/j.apcatb.2021.120470.

[4] R.P. Guan, X.Z. Yuan, Z.B. Wu, H. Wang, L.B. Jiang, J. Zhang, Y.F. Li, G.M. Zeng, D. Mo, Accelerated tetracycline degradation by persulfate activated with heterogeneous magnetic $Ni_xFe_{3-x}O_4$ catalysts, Chem. Eng. J., 350 (2018) 573–584.

[5] W.-S. Chen, Y.-C. Liu, Photocatalytic degradation of nitrobenzene in wastewater by persulfate integrated with Ag/Pb_3O_4 semiconductor under visible light irradiation, Heliyon, 7 (2021) e06984, doi: 10.1016/j.heliyon.2021.e06984.

[6] D. John, J. Jose, S.G. Bhat, V. Sivanandan Achari, Integration of heterogeneous photocatalysis and persulfate based oxidation using TiO_2-reduced graphene oxide for water decontamination and disinfection, Heliyon, 7 (2021) e07451, doi: 10.1016/j.heliyon.2021.e07451.

[7] P. Chen, Y.J. Gou, J.M. Ni, Y.M. Liang, B.Q. Yang, F.F. Jia, S.X. Song, Efficient ofloxacin degradation with Co(II)-doped MoS_2 nano-flowers as PMS activator under visible-light irradiation, Chem. Eng. J., 401 (2020) 125978, doi: 10.1016/j.cej.2020.125978.

[8] H.Y. Zhou, L.D. Lai, Y.J. Wan, Y.L. He, G. Yao, B. Lai, Molybdenum disulfide (MoS_2): a versatile activator of both peroxymonosulfate and persulfate for the degradation of carbamazepine, Chem. Eng. J., 384 (2020) 123264, doi: 10.1016/j.cej.2019.123264.

[9] Y. Chen, G. Zhang, Q.H. Ji, H.J. Liu, J.H. Qu, Triggering of low-valence molybdenum in multiphasic MoS_2 for effective reactive oxygen species output in catalytic Fenton-like reactions, ACS Appl. Mater. Interfaces, 11 (2019) 26781–26788.

[10] X.Y. Sheng, H.R. Qian, J.M. Lu, H.D. Lu, K.H. Hu, Z.H. Xu, T.T. Yu, J.S. Xie, Stepwise construction of $CdMoO_4$@CdS/MoS_2 nanocomposites for effectively visible-induced photodegradation of Rhodamine B and tetracycline, Mater. Lett., 303 (2021) 130565, doi: 10.1016/j.matlet.2021.130565.

[11] Z.P. Shi, K.Q. Nie, Z.-J. Shao, B. Gao, H.L. Lin, H.B. Zhang, B.L. Liu, Y.X. Wang, Y.H. Zhang, X.H. Sun, X.-M. Cao, P. Hu, Q.S. Gao, Y. Tang, Phosphorus-Mo_2C@Carbon nanowires toward efficient electrochemical hydrogen evolution: composition, structural and electronic regulation, Energy Environ. Sci., 10 (2017) 1262–1271.

[12] Y. Yin, J.C.. Han, Y.M. Zhang, X.H. Zhang, P. Xu, Q. Yuan, L. Samad, X.J. Wang, Y. Wang, Z.H. Zhang, P. Zhang, X.Z. Cao, B. Song, S. Jin, Contributions of phase, sulfur vacancies, and edges to the hydrogen evolution reaction catalytic activity of porous molybdenum disulfide nanosheets, J. Am. Chem. Soc., 138 (2016) 7965–7972.

[13] D.S. Baek, G.Y. Jung, B. Seo, J.C. Kim, H.-W. Lee, T.J. Shin, H.Y. Jeong, S.K. Kwak, S.H. Joo, Ordered mesoporous metastable α-MoC_{1-x} with enhanced water dissociation capability for

boosting alkaline hydrogen evolution activity, Adv. Funct. Mater., 29 (2019) 1901217, doi: 10.1002/adfm.201901217.
[14] B. Sheng, F. Yang, Y.H. Wang, Z.H. Wang, Q. Li, Y.G. Guo, X.Y. Lou, J.S. Liu, Pivotal roles of MoS_2 in boosting catalytic degradation of aqueous organic pollutants by Fe(II)/PMS, Chem. Eng. J., 375 (2019) 121989, doi: 10.1016/j.cej.2019.121989.
[15] X.Y. Li, Y.M. Wang, Z.D. Pan, Effects of solution pH value and mineralizer on formation and color property of holmium molybdate pigment *via* co-precipitation and sintering, Ceram. Int., 47 (2021) 5677–5689.
[16] Y. Chen, G. Zhang, H.J. Liu, J.H. Qu, Confining free radicals in close vicinity to contaminants enables ultrafast Fenton-like processes in the interspacing of MoS_2 membranes, Angew. Chem. Int. Ed, 58 (2019) 8134–8138.
[17] C.L. Yu, H.B. Hu, X.Q. Liu, J.L. Zeng, Z. Liu, Novel SiO_2 nanoparticle-decorated BiOCl nanosheets exhibiting high photocatalytic performances for the removal of organic pollutants, Chin. J. Catal., 40 (2019) 1212–1221.
[18] X.H. Li, S.D. Deng, H. Fu, G.N. Mu, Synergistic inhibition effect of rare earth cerium(IV) ion and sodium oleate on the corrosion of cold rolled steel in phosphoric acid solution, Corros. Sci., 52 (2010) 1167–1178.
[19] Y.W. Tang, J.K. Wang, M. Wang, C.Y. Jin, J.Y. Liu, M. Li, S.Y. Li, Z.L. Li, Catalytic degradation of oxytetracycline via $FeVO_4$ nanorods activating PMS and the insights into the performance and mechanism, J. Environ. Chem. Eng., 9 (2021) 105864, doi: 10.1016/j.jece.2021.105864.
[20] X.G. Li, Y.X. Guo, L.G. Yan, T. Yan, W. Song, R. Feng, Y.W. Zhao, Enhanced activation of peroxymonosulfate by ball-milled MoS_2 for degradation of tetracycline: boosting molybdenum activity by sulfur vacancies, Chem. Eng. J., 429 (2022) 132234, doi: 10.1016/j.cej.2021.132234.
[21] Z.Y. Wang, A. von dem Bussche, Y. Qiu, T.M. Valentin, K. Gion, A.B. Kane, R.H. Hurt, Chemical dissolution pathways of MoS_2 nanosheets in biological and environmental media, Environ. Sci. Technol., 50 (2016) 7208–7217.
[22] Y.-T. Lin, C.J. Liang, J.-H. Chen, Feasibility study of ultraviolet activated persulfate oxidation of phenol, Chemosphere, 82 (2011) 1168–1172.
[23] H.Y. Zhou, J.L. Peng, J.Y. Li, J.J. You, L.D. Lai, R. Liu, Z.M. Ao, G. Yao, B. Lai, Metal-free black-red phosphorus as an efficient heterogeneous reductant to boost Fe^{3+}/Fe^{2+} cycle for peroxymonosulfate activation, Water Res., 188 (2021) 116529, doi: 10.1016/j.watres.2020.116529.
[24] Y.X. Liu, Y. Wang, Q. Wang, J.F. Pan, J. Zhang, Simultaneous removal of NO and SO_2 using vacuum ultraviolet light (VUV)/heat/peroxymonosulfate (PMS), Chemosphere, 190 (2018) 431–441.
[25] G. Lente, J. Kalmár, Z. Baranyai, A. Kun, I. Kék, D. Bajusz, M. Takács, L. Veres, I. Fábián, One- versus two-electron oxidation with peroxomonosulfate ion: reactions with iron(II), vanadium(IV), halide ions, and photoreaction with cerium(III), Inorg. Chem., 48 (2009) 1763–1773.